Available online at www.sciencedirect.com
ScienceDirect
International Journal of Multiphase Flow 33 (2007) 411–431
International Journal of Multiphase Flow
www.elsevier.com/locate/ijmulflow

Two-phase flow in a horizontal equal-sided impacting tee junction

A.M.F. El-Shaboury, H.M. Soliman *, G.E. Sims

Department of Mechanical and Manufacturing Engineering, University of Manitoba, Winnipeg, Manitoba, Canada R3T 5V6

Received 20 April 2006; received in revised form 27 September 2006

Abstract

Pressure-drop and phase-distribution data were generated for air–water flows in a horizontal impacting tee junction. All three sides of the junction (37.8-mm i.d.) were oriented horizontally. The data correspond to a junction pressure of 1.5 bar (abs), ambient temperature, inlet flow regimes of wavy, stratified, and annular, and a wide range of mass splits at the junction. Most of the range for the phase-distribution data corresponds to conditions that were untested in previous investigations. In general, it was found that the phases did not distribute themselves evenly between the two outlets unless the mass split is equal. There is a serious lack of data in the literature on the two-phase pressure drop in impacting tee junctions and therefore, the present data add substantially to the existing data. A mechanistic model capable of predicting the phase distribution and pressure drop was developed and shown to be in general good agreement with the present data and others from the literature.

Keywords: Impacting tee junction; Gas–liquid flow; Experimental; Pressure drop; Phase distribution; Modelling

1. Introduction

Two-phase flow commonly occurs in many systems in the power and process industries, such as conventional steam power plants, evaporators and condensers, boiling-water and pressurized-water nuclear reactors, and a wide variety of chemical and petroleum applications. Quite often, the complex piping networks in these systems require the two-phase flow to pass through tee junctions. Tee junctions may be used to combine two inlet streams into one outlet stream (combining tees) or to divide one inlet stream into two outlet streams (dividing tees). For the case of dividing tees, a tee junction may have one of two different configurations: branching or impacting. For the case of branching tees, one of the two outlet streams is in the same direction as the inlet and the other outlet is perpendicular to the inlet. For the case of impacting tees, the two outlet streams have opposite directions and both are perpendicular to the inlet. The three sides of an impacting

* Corresponding author. Tel.: +1 204 474 9307; fax: +1 204 275 7507.
E-mail address: hsolima@cc.umanitoba.ca (H.M. Soliman).

0301-9322/$ - see front matter © 2006 Elsevier Ltd. All rights reserved.
doi:10.1016/j.ijmultiphaseflow.2006.10.002

tee junction may have different orientations between two limiting positions: vertically upward and vertically downward. In this study, the focus is on impacting tee junctions with three horizontal sides.

When a two-phase flow passes through an impacting tee, mal-distribution of the phases may occur; i.e., the qualities of the mixtures in both outlets downstream from the junction are not equal to the inlet quality. Certain mass split ratios can lead to single-phase gas flowing in one of the outlets (with both gas and liquid flowing in the other outlet), while other split ratios can lead to single-phase liquid flowing in one of the outlets (with both gas and liquid flowing in the other outlet); these conditions will be treated later as part of the discussion on phase-split behavior. This severe mal-distribution of the phases can have a significant effect on the operation and efficiency of components downstream from the junction. Therefore, it is very important to be able to predict the manner by which the two phases distribute themselves at impacting tees for different operating conditions. Another important parameter is the pressure change experienced by the flow solely due to the existence of the junction. This pressure change is normally expressed in terms of two pressure drops: the inlet-to-outlet-2 and inlet-to-outlet-3 pressure drops, ΔP_{12} and ΔP_{13}, respectively.

A few studies have been reported in the literature on the phase distribution in horizontal impacting tees. These include the experiments by Hong (1978); Hwang et al. (1989); Chien and Rubel (1992); Ottens et al. (1995); Hong and Griston (1995); Fujii et al. (1995) and Asano et al. (1997). All these studies used equal-sided tees with inside diameters ranging from 9.5 to 49.3 mm. The two-phase mixtures used were air–water, nitrogen-water, steam-water, or saturated vapour-liquid mixtures of refrigerant R-11. The system pressure in these studies was at or near atmospheric, except for the work of Chien and Rubel with steam-water at a system pressure of 28.6–42.4 bar. A fairly wide range of mass splits was tested in these experiments. With the exception of the study by Hong, all other studies concluded that generally the phases do not split evenly at the junction, i.e., the two outlet qualities are different and they are both different from the inlet quality, except at the condition of even mass split. The manner by which the phases distribute themselves at the junction was found to depend in a complicated fashion on the inlet conditions, fluid properties, and total mass split at the junction. No pressure-drop measurements were reported in these studies.

For impacting tees with a vertical inlet and horizontal outlets, phase distribution data were generated for an inlet flow regime of annular flow (Azzopardi et al., 1986a) and churn flow (Azzopardi et al., 1986b). The conclusions about the mal-distribution of the phases and the dependence of the phase distribution on the inlet conditions as well as the mass split at the junction were similar to those obtained for horizontal junctions. Recent reviews of the literature on the phase distribution in tee junctions can be found in Azzopardi (1999) and El-Shaboury et al. (2001).

To the best of the authors' knowledge, the only pressure-drop data available in the literature for two-phase flow in impacting tees are those reported by Hwang (1986). These data correspond to inlet flow regimes of bubbly and bubbly-stratified flows. Reference will be made later on to the single-phase pressure-drop results from this study; however, the two-phase conditions tested by Hwang are considerably different from the present conditions.

The literature survey indicates that the range of inlet conditions covered in the previous phase-distribution studies is limited. Since the phase-distribution phenomenon is strongly dependent on the inlet conditions, the need for further data is obvious. In addition, a broader data base provides a solid foundation for modelling. The need for pressure-drop data is even more urgent given that only one data set is currently available. The present study has been conducted to generate experimental data on the phase distribution and pressure drop for air–water mixtures through a horizontal impacting tee junction. The data cover a wide range of inlet conditions that so far have been untested, including high-inlet-quality mixtures. Another objective of the current study is to develop a model/correlation for predicting the phase split and pressure drop during two-phase flow in horizontal impacting tees.

2. Experimental investigation

2.1. Flow loop

The flow loop that was designed and constructed for this study is shown schematically in Fig. 1. Distilled water used in the system was stored in the water reservoir. Water was fed from the reservoir by a centrifugal

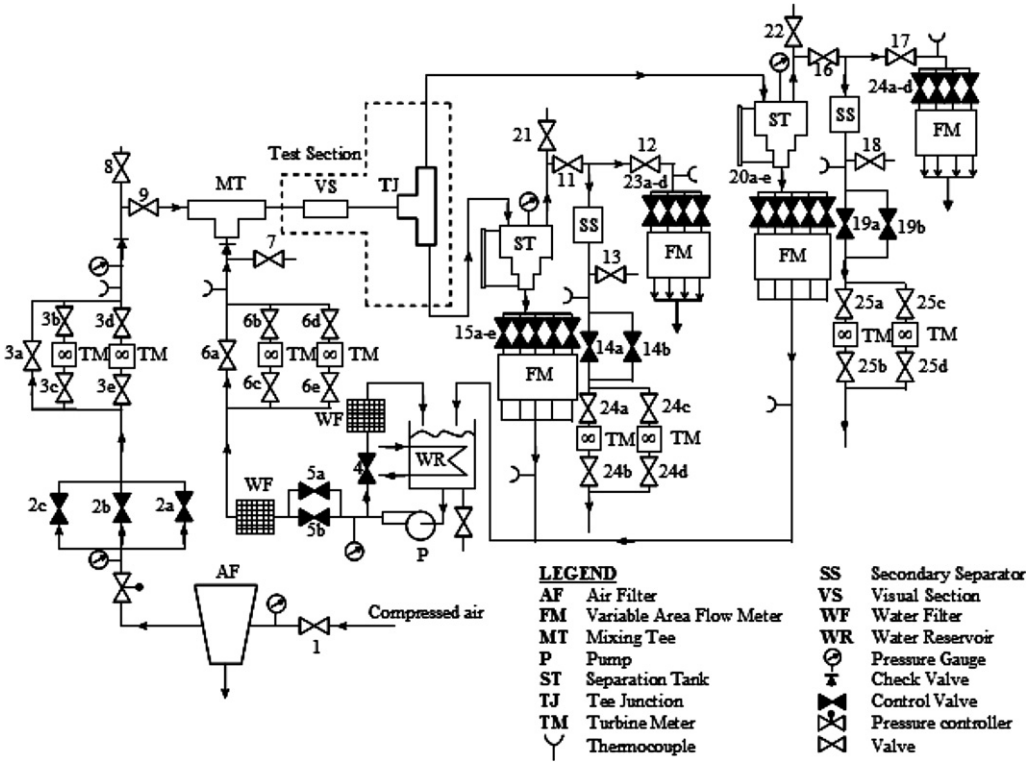

Fig. 1. Schematic diagram of the experimental facility.

pump equipped with a by-pass line and then mixed with air supplied from an air compressor in the two-phase mixing tee (mixer). A cooling coil installed inside the reservoir removed heat absorbed by the water due to flow through the pump and from frictional losses. Necessary equipment was installed on the water and air supply lines to allow for pressure and flow-rate control, as well as filtering of both streams. A developing length of 67.5 tube diameters was allowed before the two-phase mixture entered a visual section, and a further 66 tube diameters was provided before entering the tee junction which was made from acrylic for visualization. The two-phase mixtures emerging from the junction were directed to their respective separation tank. All sides of the test section (the inlet side between the mixer and the tee junction and the two outlet sides, namely outlet 2 and outlet 3, from the junction to their respective separation tank) were horizontal. In the separation tanks, the individual flows of air and water were separated and then measured. Water flows from the separation tanks were rejoined and returned to the water reservoir, while both air streams were discharged into the atmosphere. The piping used for the construction of the test section was special-order copper tubing with inside diameter $D = 37.8$ mm and outside diameter 41.3 mm. A differential water level (accurate to 1.5 mm) was used to ensure horizontality of the test section. Extreme care was taken in order to ensure that the entire test facility (up to the separation tanks) was symmetric around the inlet centreline. Control of the total mass split at the junction for both single-phase and two-phase experiments was by means of the control valves downstream of the separation tanks.

2.2. Instrumentation

The inlet water mass flow rate, W_{L1}, was metered using one of two turbine meters with overlapping ranges. The water mass flow rates from outlets 2 and 3, W_{L2} and W_{L3}, respectively, were metered using two separate banks, each with five rotameters having overlapping ranges. The inlet air mass flow rate, W_{G1}, was metered using one of two turbine meters with overlapping ranges. The air mass flow rates through outlets 2 and 3, W_{G2} and W_{G3}, respectively, were metered by two separate measuring stations, each consisting of two turbine meters

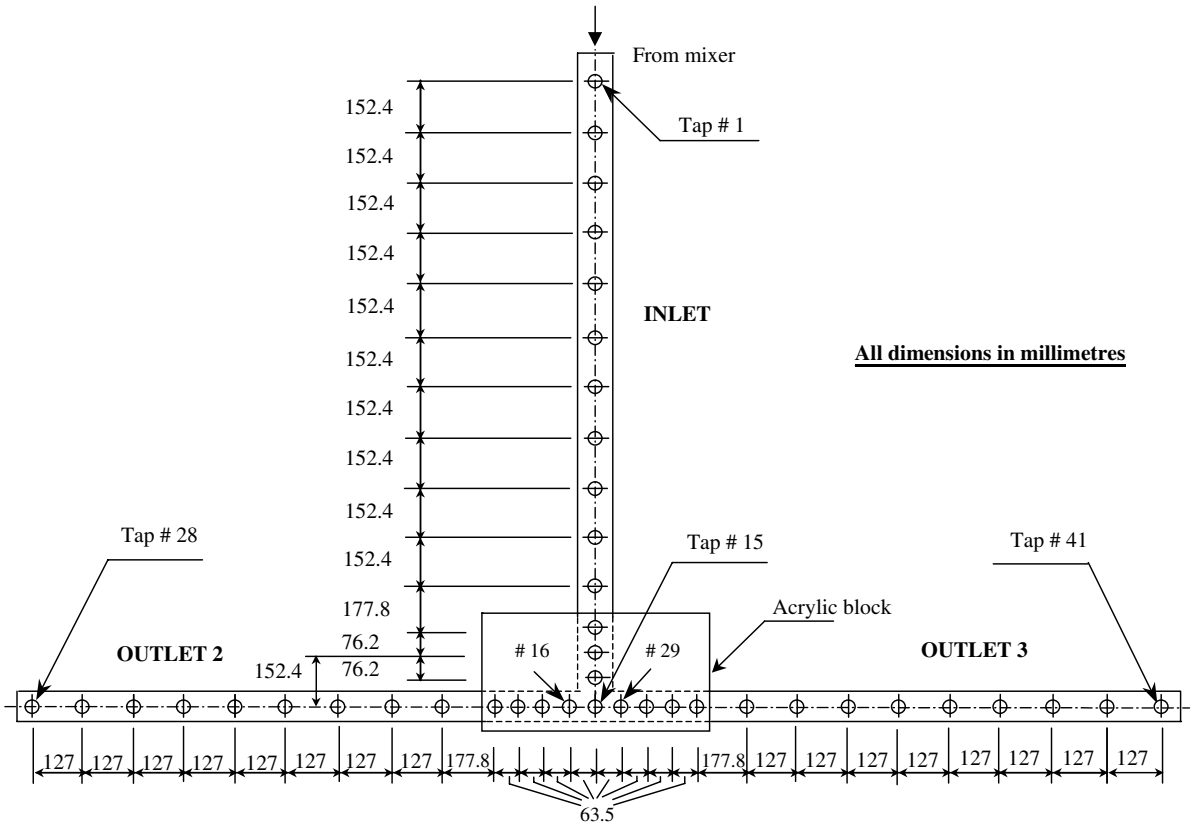

Fig. 2. Locations of pressure taps.

with overlapping ranges (for high flow rates) and a bank of four rotameters with overlapping ranges (for low flow rates). All rotameters and turbine meters were calibrated in the laboratory.

A total of 41 pressure taps were installed along the whole test section, as shown in Fig. 2. The pressure taps were located along the bottom side of the test section and were connected by means of water-filled plastic tubing to the pressure-measurement station, at which the pressure distribution across the 41 taps was measured. This station consisted of two identical banks of pressure transducers, each bank consisting of four Rosemount transducers with overlapping ranges. The system pressure, P_s, was defined as the absolute pressure at the centre of the tee junction (tap number 15 in Fig. 2) and was measured using a separate Rosemount transducer. All pressure transducers were calibrated in the laboratory. Care was taken that no air was trapped in the pressure lines during measurement.

The data-acquisition system, with components generally by National Instruments Corporation, consisted of a multifunction I/O board with its driving software, shielded connector block, shielded cable, and data-acquisition software. The DC voltage signals coming from the turbine meters, thermocouples, and pressure transducers were digitised and averaged for 120 s at a rate of 1000 samples per second. The calibration data relevant to the various instruments were applied.

2.3. Data reduction

Using the measured values of W_{L1}, W_{L2}, W_{L3}, W_{G1}, W_{G2} and W_{G3}, the inlet, outlet 2, and outlet 3 total mass flow rates, W_1, W_2 and W_3, respectively, were obtained. Also, the inlet, outlet 2, and outlet 3 qualities, x_1, x_2 and x_3, respectively, were obtained from the definition $x_i = W_{Gi}/W_i$, $i = 1, 2, 3$. The superficial liquid velocities were calculated from $J_{Li} = 4W_{Li}/(\pi\rho_L D_i^2)$, $i = 1, 2, 3$, where ρ_L is the liquid density, and the superficial gas velocities were calculated from $J_{Gi} = 4W_{Gi}/(\pi\rho_G D_i^2)$, $i = 1, 2, 3$, where ρ_G is the gas density. The fraction

of total inlet gas diverted through outlet 3, F_{BG}, and the fraction of total inlet liquid diverted through outlet 3, F_{BL}, were calculated from $F_{BG} = W_{G3}/(W_{G2} + W_{G3})$ and $F_{BL} = W_{L3}/(W_{L2} + W_{L3})$, respectively.

Using the scanned pressure distribution from the 41 pressure taps, linear equations were fitted to the fully-developed data in the inlet and the two outlets using the least-squares analysis. Details of this analysis are outlined in El-Shaboury (2005). By extrapolating the fully-developed pressure gradients in the inlet and the outlets to the centre of the tee junction, the inlet, outlet 2, and outlet 3 junction average pressures, P_1, P_2, and P_3, respectively, were determined. Using the three junction average pressures, values of the pressure drops (ΔP_{12} and ΔP_{13}) were determined from $\Delta P_{12} = P_1 - P_2$ and $\Delta P_{13} = P_1 - P_3$.

2.4. Experimental uncertainty

Overall mass balances were performed individually on both the air and water streams. The mass-balance errors were defined as the percentage deviation between the inlet flow rate of a specific phase and the sum of its outlet flow rates. The air mass-balance error was within ±3.5% for 66% of the data and all the data were within ±5.3%. The water mass-balance error was within ±3.5% for 70% of the data and all the data were within ±5.2%.

An uncertainty analysis was conducted based on the methods of Kline and McClintock (1953) and Moffat (1988). All uncertainties given in the current study are at "odds" (as used by the above-given authors) of 20:1. The uncertainties are meant to accommodate: discrimination uncertainties in the measuring instruments, the error in fitting an equation to the calibration data, and the accuracy of the calibrating devices.

The uncertainties in the values of J_{G1}, J_{L1}, and x_1 were found to be within ±4.4% and the uncertainty in P_s was found to be within ±1%. For W_3/W_1, x_3/x_1, F_{BG}, and F_{BL}, the uncertainties were within ±11.7%. For ΔP_{12} and ΔP_{13}, 82% of the data had uncertainties within ±30%. In a few test runs, where the value of ΔP_{12} or ΔP_{13} was very small, very large uncertainty values were found. In these tests, the uncertainty in the individual values of P_1, P_2, and P_3 were very small (typically <3%). However, because the values of ΔP_{12} or ΔP_{13} were very small relative to the values of P_1, P_2, and P_3, the uncertainty values of ΔP_{12} or ΔP_{13} became very large.

3. Experimental results and discussion

3.1. Single-phase pressure drop

A total of 18 single-phase-flow test runs were performed. Fourteen of these runs were performed using air and the remaining four were performed using water. For the air runs, two nominal inlet-air velocities were tested, namely 20 and 40 m/s, and the test-section pressure was kept nominally at 1.5 bar. These conditions corresponded to inlet Reynolds numbers, Re, of 72,850 and 145,700, where $Re = \rho V_1 D_1/\mu$, V_1 is the average inlet velocity and μ is the viscosity. The extraction ratio (W_3/W_1) was varied over the range 0.0–1.0. For the water runs, the nominal inlet-water velocity was 0.18 m/s, the test-section pressure was within 1.04–1.1 bar, and the extraction ratio (W_3/W_1) was set to 0.0, 0.1, 0.9, and 1.0. These conditions corresponded to $Re = 7170$ for the water.

For single-phase flow, the Bernoulli equation (with the loss term included) between the inlet and outlet 3 yields the following:

$$\Delta P_{13} = P_1 - P_3 = \rho\left(\frac{V_3^2}{2} - \frac{V_1^2}{2}\right) + (P_1 - P_3)_{irr} \tag{1}$$

where V_1 and V_3 are the average inlet and outlet-3 velocities, respectively, and $(P_1 - P_3)_{irr}$ is the irreversible component of ΔP_{13}, given by

$$(P_1 - P_3)_{irr} = K_{13}(\rho V_1^2/2) \tag{2}$$

where K_{13} is the pressure loss coefficient between the inlet and outlet 3.

Similarly, the pressure drop ΔP_{12} can be expressed as

$$\Delta P_{12} = P_1 - P_2 = \rho\left(\frac{V_2^2}{2} - \frac{V_1^2}{2}\right) + K_{12}(\rho V_1^2/2) \tag{3}$$

The current single-phase-flow pressure-drop data were used to calculate the pressure loss coefficient K_{13} and its counterpart for outlet 2, K_{12}, using Eqs. (1)–(3). Fig. 3 shows the variation of K_{13} with the extraction ratio W_3/W_1 for the two nominal air velocities and the nominal water velocity. The empirical correlation developed by Ito and Imai (1973), which was based on data for water over the range $100{,}000 \leqslant Re \leqslant 200{,}000$, and the correlation developed by Hwang (1986) for the coefficient K_{13} are also shown in the figure. Also in the figure, values of K_{12} evaluated at (W_2/W_1) are shown in order to test the symmetry of the test section. The figure shows that values of K_{13} at W_3/W_1 and those of K_{12} at (W_2/W_1) are very close to each other, which is evidence of the symmetry of the test section. It can also be seen that, for the two different air velocities and the liquid velocity, values of K_{13} and K_{12} are very close to each other. The present experimental data agree very well with the correlation of Ito and Imai (1973) over the whole correlation range. However, the empirical correlation by Hwang does not follow the experimental-data trend of Ito and Imai or the present investigation. Fig. 3 suggests that values of the single-phase pressure loss coefficients K_{12} and K_{13} are dependent only on the extraction ratio W_3/W_1. No dependence on the fluid properties or the inlet Reynolds number is observed within the tested range.

3.2. Two-phase data range

The two-phase pressure distribution data generated in this experimental investigation consist of 11 data sets. Each data set corresponds to a fixed combination of J_{G1} and J_{L1} but different extraction ratios, W_3/W_1. A total of 55 test runs were performed with 10 more runs performed for repeatability purposes. The nominal test-section pressure was 1.5 bar (abs) and the average test-section temperature was 23.5 °C. The nominal values of J_{G1} and J_{L1} for the 11 data sets generated are shown in Fig. 4 on the flow-regime map of Mandhane et al. (1974). For future reference, the data sets in Fig. 4 are labelled according to the observed inlet flow regime. The observed flow regimes were consistent with the classification shown on the map of Fig. 4. The standard descriptions were used in identification of the major flow regimes, while the transitional flow regime of stratified-wavy was identified using the description given in Buell et al. (1994).

3.3. Two-phase pressure drop

Samples of the pressure-distribution data for different inlet flow regimes are shown in Figs. 5 and 6. These data are presented on graphs of $(P - P_r)$ versus the distance from the junction centre, where P is the absolute local pressure and P_r is a reference pressure (the absolute pressure at tap 1, see Fig. 2). Fig. 5 shows pressure-distribution data for data set A1 with $W_3/W_1 = 0.5$. The figure shows that the pressure distributions in the two

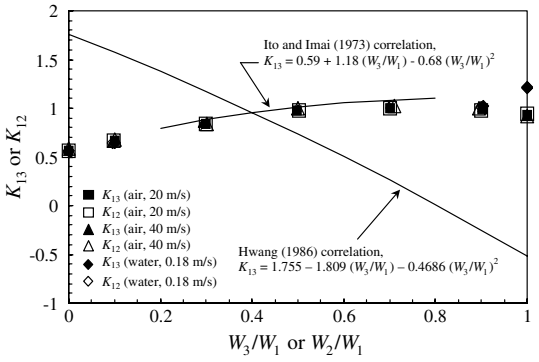

Fig. 3. Single-phase loss coefficients, K_{13} and K_{12}.

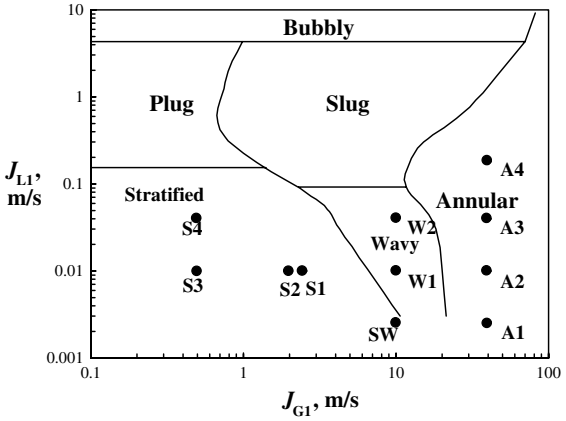

Fig. 4. The inlet flow conditions on the Mandhane et al. (1974) flow-regime map.

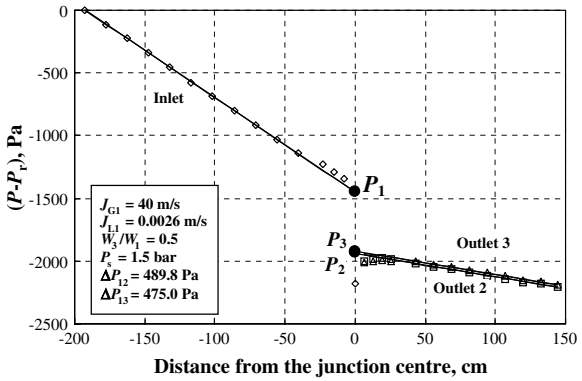

Fig. 5. Pressure distribution for data set A1 with $W_3/W_1 = 0.5$.

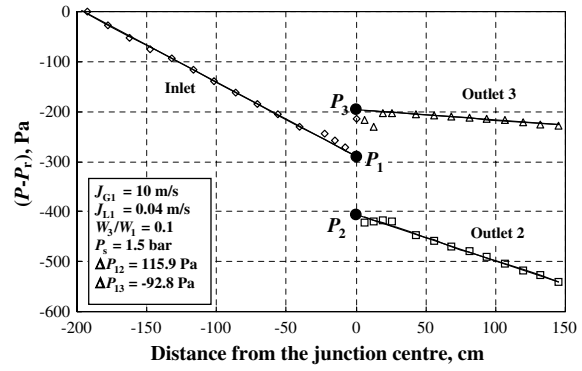

Fig. 6. Pressure distribution for data set W2 with $W_3/W_1 = 0.1$.

outlets are very close to each other, which is further evidence of the symmetry of the tee junction around the inlet centreline. As a result, values of ΔP_{12} and ΔP_{13} are close to each other with a percentage difference of 3%. Another pressure-distribution sample is shown in Fig. 6 for data set W2 with $W_3/W_1 = 0.1$. An observation on Figs. 5 and 6 is that the measured pressure drop at all taps in the inlet side remained close to the fully developed behaviour. This observation is important as we look at the stratified-flow data next.

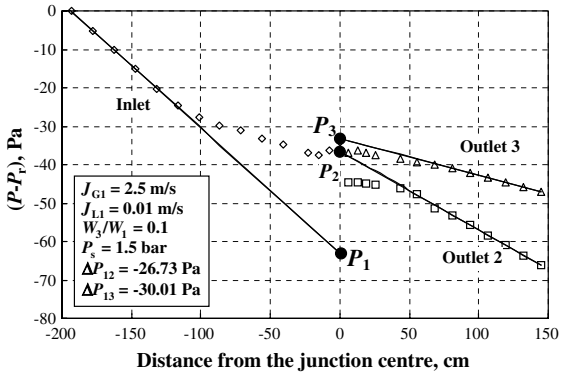

Fig. 7. Pressure distribution for data set S1 with $W_3/W_1 = 0.1$.

Fig. 7 shows the pressure-distribution data for set S1 with $W_3/W_1 = 0.1$. This figure shows that the pressure-drop values (ΔP_{12} and ΔP_{13}) are considerably smaller than those for wavy and annular flows; actually, the difference between the highest pressure and the lowest pressure in Fig. 7 is about 65 Pa. This observation was found to be consistent in all the data of stratified flow. Another observation is that the pressure-data in the inlet deviate from the linear behaviour at a large distance from the junction centre (approximately 120 cm in Fig. 7). This observation was also found to be consistent in all the data of stratified flow; however, the location at which the data start to deviate from the linear behaviour was found to vary with the inlet conditions. Fig. 8 shows pressure-distribution data for sets S1–S4 with $W_3/W_1 = 0.5$. This figure shows that the location at which the data start to deviate from the linear behaviour in the inlet varies with the inlet conditions, with J_{G1} being the dominant factor (compared with J_{L1}) in determining that location. The figure also provides another confirmation of the symmetry of the junction by showing that the data in the two outlets are close to each other for all the data sets at the condition of even mass split.

A possible reason for the deviation of the inlet pressure-drop data from the linear behaviour was investigated. Visual observations aided by a high-speed video camera revealed that there is a swelling of the interface level at the junction (El-Shaboury, 2005). The fact that the interface height swells at the junction may be explained by looking at the junction as an obstruction to the incoming flow and realizing that the small interfacial shear (due to the low value of J_{G1}) is not able to smooth out this swelling. These visual observations were found to be common to all stratified-flow data; however, it was found that the magnitude and shape of the interface swelling at the junction varied with the inlet conditions and the split ratio.

The above mentioned visual observations, together with the pressure measurements shown in Figs. 7 and 8 gave rise to the question about the effect of the interface level in all three sides of the junction on the magnitude and form of the pressure distribution. A difference in elevation of 2 mm results in a 20 Pa pressure difference,

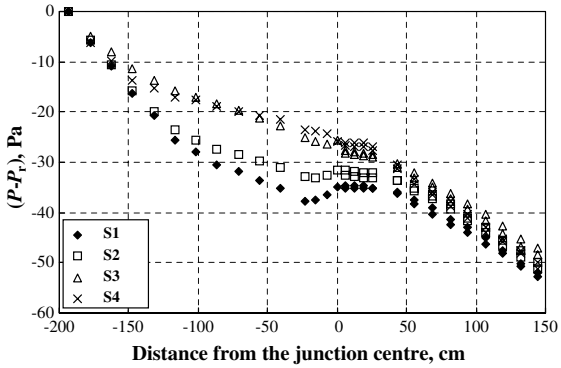

Fig. 8. Pressure distribution for data sets S1 to S4 with $W_3/W = 0.5$.

Table 1
Phase-distribution and pressure-drop data

Test	J_{G1} (m/s)	J_{L1} (m/s)	P_s (bar)	T_1 (°C)	x_1 (%)	W_3/W_1	F_{BG}	F_{BL}	ΔP_{12} (Pa)	ΔP_{13} (Pa)
S1-1	2.50	0.0100	1.50	21.6	30.8	0.000	0.000	0.000		
S1-2	2.49	0.0105	1.50	21.4	29.5	0.000	0.000	0.000		
S1-3	2.50	0.0100	1.52	23.8	30.9	0.100	0.000	0.144		
S1-4	2.50	0.0100	1.50	21.5	30.8	0.115	0.027	0.156		
S1-5	2.50	0.0101	1.49	22.4	30.5	0.281	0.239	0.299		
S1-6	2.48	0.0097	1.50	21.6	31.2	0.487	0.499	0.482		
S1-7	2.50	0.0100	1.50	21.6	30.8	0.499	0.499	0.499		
S2-1	2.00	0.0101	1.50	21.7	26.1	0.000	0.000	0.000		
S2-2	1.96	0.0100	1.50	21.6	25.9	0.180	0.000	0.243		
S2-3	2.04	0.0097	1.51	21.6	27.5	0.342	0.262	0.371		
S2-4	2.00	0.0099	1.51	21.4	26.5	0.500	0.502	0.499		
S3-1	0.50	0.0101	1.52	21.7	8.19	0.000	0.000	0.000		
S3-2	0.49	0.0098	1.52	21.4	8.27	0.429	0.163	0.454		
S3-3	0.51	0.0097	1.51	21.5	8.63	0.398	0.000	0.437		
S3-4	0.48	0.0100	1.51	21.4	7.93	0.488	0.506	0.487		
S3-5	0.50	0.0100	1.51	21.4	8.23	0.499	0.499	0.499		
S4-1	0.50	0.0403	1.51	21.8	2.16	0.000	0.000	0.000		
S4-2	0.50	0.0404	1.51	21.5	2.16	0.466	0.000	0.477		
S4-3	0.49	0.0395	1.50	21.6	2.15	0.491	0.500	0.491		
S4-4	0.50	0.0400	1.50	21.5	2.17	0.498	0.501	0.497		
SW-1	10.01	0.0026	1.50	22.0	87.1	0.000	0.000	0.000	84.2	−48.4
SW-2	10.00	0.0026	1.51	24.9	87.0	0.097	0.111	0.001	33.1	−41.4
SW-3	10.03	0.0027	1.51	24.0	87.0	0.097	0.111	0.001	29.8	−45.4
SW-4	10.00	0.0026	1.50	22.5	87.2	0.307	0.347	0.029	6.6	−39.0
SW-5	10.00	0.0026	1.49	25.3	87.0	0.294	0.338	0.001	5.7	−36.9
SW-6	10.00	0.0026	1.50	25.3	87.0	0.401	0.437	0.155	−8.3	−36.5
SW-7	10.00	0.0026	1.50	23.6	87.1	0.501	0.501	0.499	−18.4	−16.7
SW-8	10.02	0.0026	1.50	24.0	87.0	0.500	0.500	0.499	−18.7	−17.9
W1-1	10.03	0.0101	1.51	21.4	63.9	0.000	0.000	0.000	109.7	−27.6
W1-2	10.01	0.0104	1.50	24.9	62.8	0.037	0.043	0.026	69.8	−41.5
W1-3	10.03	0.0102	1.50	21.5	63.5	0.099	0.107	0.087	71.5	−54.5
W1-4	10.02	0.0103	1.50	21.3	63.4	0.299	0.311	0.281	22.2	−41.3
W1-5	9.97	0.0102	1.50	21.6	63.4	0.497	0.496	0.497	−24.8	−22.7
W1-6	10.02	0.0104	1.51	21.6	63.3	0.703	0.690	0.723	−43.5	21.3
W2-1	10.04	0.0406	1.50	21.0	30.6	0.000	0.000	0.000	157.2	−82.9
W2-2	10.00	0.0403	1.50	23.1	30.6	0.049	0.000	0.070	134.6	−87.6
W2-3	10.00	0.0406	1.50	21.2	30.5	0.109	0.028	0.144	115.9	−92.8
W2-4	10.03	0.0403	1.50	21.2	30.7	0.300	0.234	0.329	58.9	−76.7
W2-5	10.04	0.0404	1.50	20.5	30.8	0.300	0.234	0.330	58.5	−77.2
W2-6	9.99	0.0402	1.50	21.5	30.7	0.502	0.496	0.505	−24.9	−27.2
W2-7	10.04	0.0403	1.51	23.5	30.6	0.503	0.503	0.503	−27.7	−27.1
A1-1	40.01	0.0027	1.51	25.3	96.4	0.000	0.000	0.000	1583	−604.2
A1-2	39.99	0.0026	1.50	25.5	96.4	0.101	0.104	0.001	1358	−473.9
A1-3	40.01	0.0026	1.51	28.5	96.4	0.196	0.201	0.001	1044	−209.4
A1-4	40.01	0.0026	1.50	26.4	96.4	0.338	0.343	0.166	766.4	8.3
A1-5	40.03	0.0026	1.51	25.2	96.4	0.495	0.495	0.500	489.8	475.0
A2-1	39.99	0.0104	1.51	26.5	87.1	1.000	1.000	1.000	−663.0	1742
A2-2	39.93	0.0104	1.50	23.3	87.2	1.000	1.000	1.000	−665.2	1752
A2-3	40.00	0.0099	1.51	26.2	87.6	0.045	0.043	0.062	1548	−662.3
A2-4	40.00	0.0100	1.50	26.5	87.5	0.099	0.092	0.152	1409	−539.1
A2-5	40.00	0.0102	1.51	24.9	87.4	0.300	0.295	0.334	1013	−118.9
A2-6	39.98	0.0101	1.50	24.0	87.5	0.503	0.503	0.501	395.1	408.2

(*continued on next page*)

Table 1 (*continued*)

Test	J_{G1} (m/s)	J_{L1} (m/s)	P_s (bar)	T_1 (°C)	x_1 (%)	W_3/W_1	F_{BG}	F_{BL}	ΔP_{12} (Pa)	ΔP_{13} (Pa)
A3-1	39.94	0.0406	1.51	27.0	63.3	1.000	1.000	1.000	−949.4	2538
A3-2	39.91	0.0404	1.52	24.3	63.7	1.000	1.000	1.000	−988.3	2625
A3-3	39.89	0.0409	1.49	28.3	62.8	0.962	1.000	0.900	−851.4	2283
A3-4	40.00	0.0399	1.51	22.6	64.1	0.118	0.049	0.241	1995	−768.2
A3-5	40.01	0.0399	1.51	22.7	64.1	0.309	0.267	0.385	1106	−302.9
A3-6	40.04	0.0399	1.51	24.7	63.9	0.503	0.505	0.500	217.6	238.6
A4-1	39.45	0.1795	1.52	20.7	28.4	1.000	1.000	1.000	−1482	6881
A4-2	39.52	0.1795	1.51	22.2	28.3	0.923	1.000	0.892	−1245	6872
A4-3	39.71	0.1800	1.50	24.6	28.0	0.806	0.989	0.735	−1142	6614
A4-4	39.55	0.1798	1.51	27.3	27.9	0.744	0.899	0.683	−1048	4236
A4-5	40.07	0.1808	1.50	21.6	28.3	0.399	0.320	0.430	1451	−100.1
A4-6	40.00	0.1807	1.51	22.8	28.2	0.503	0.505	0.502	469.2	468.8
A4-7	40.09	0.1809	1.51	24.8	28.2	0.498	0.498	0.499	471.4	449.8

which is significant when the difference between the highest and lowest pressures is 65 Pa. On the other hand, differences in elevation have little impact in annular and wavy flows because of the much higher pressure differences. Therefore, it was concluded that the small changes in the interface level among the three sides of the junction during stratified flow and the significant effects that these may have on the shape and magnitude of the pressure-distribution data would result in significant errors in determining the values of ΔP_{12} and ΔP_{13}. As a result, it was decided not to report any pressure-drop data (ΔP_{12} and ΔP_{13}) for the stratified flow; however, all the current pressure-distribution data for stratified flow are available in El-Shaboury (2005). The measured values of ΔP_{12} and ΔP_{13}, together with the corresponding operating conditions for the stratified-wavy, wavy, and annular test runs are listed in Table 1.

3.4. Assessment of the measured fully-developed pressure gradients

The average fully-developed pressure gradients measured in the inlet side of the junction during the single-phase tests were compared against the calculated values from Moody's diagram for smooth tubes. Good agreement was found between the two sets of values for both air and water with a maximum percentage deviation of 7.8%.

For the two-phase tests, the average fully-developed pressure gradients measured in the inlet side of the junction were compared against the predictions of the correlations proposed by Lockhart and Martinelli (1949) and Chisholm (1967). This was done for all the experiments of the wavy, stratified-wavy, and annular flow regimes. In addition, the pressure gradients for the experiments of the wavy and stratified-wavy flow regimes were compared against the model of Grolman and Fortuin (1997). The correlation of Lockhart and Martinelli (1949) gave the best predictions of the pressure gradients for annular flow with an average percentage difference of 15.5%. For wavy and stratified-wavy flows, the predictions of Chisholm (1967) gave the best agreement with a maximum percentage difference of 15.0%.

3.5. Phase distribution

The phase-distribution data obtained from this study are presented on graphs of F_{BL} versus F_{BG}. In these graphs, the data points shown for ranges of F_{BG} and F_{BL} from 0.0 to 0.5 are the actual measurements for outlet 3. The data points shown for the ranges from 0.5 to 1.0 are the actual measurements for outlet 2 but were used in the graphs for outlet 3 based on symmetry.

Fig. 9 shows the phase-distribution data for the stratified flow regime. It can be seen that for the four data sets there is a preference for the liquid phase to exit through outlet 3 (i.e., $F_{BL} > F_{BG}$) over the range $0.0 < F_{BG} < 0.5$. This can be translated into x_3/x_1 values that are less than 1.0 over the range $0.0 < W_3/W_1 < 0.5$. In the range $0.5 < F_{BG} < 1.0$, the gas phase has a preference to go through outlet 3 (i.e., $F_{BG} > F_{BL}$). This can be translated into x_3/x_1 values that are higher than 1.0 over the range $0.5 < W_3/W_1 < 1.0$. It should be

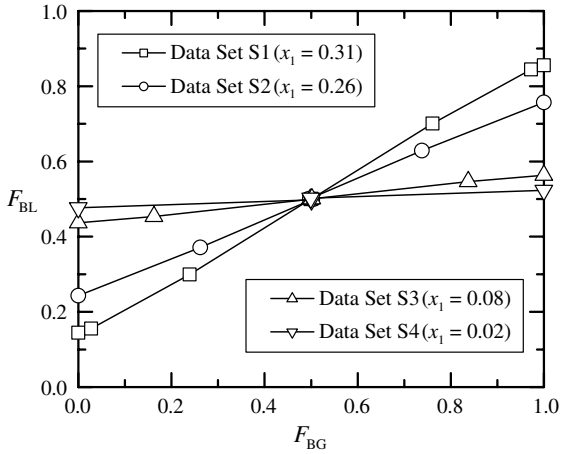

Fig. 9. Phase-distribution data for the stratified flow regime.

noted that data sets S1, S2, S3, and S4 have inlet-quality values of 0.31, 0.26, 0.08, and 0.02, respectively. Fig. 9 shows that there is a continuous trend in the data such that as x_1 decreases, the data line (or curve) moves around the point (0.5, 0.5) in a clockwise direction. El-Shaboury (2005) pointed out that the data should approach the line $F_{BL} = 0.5$ as x_1 approaches zero and the data should approach the line $F_{BG} = 0.5$ as x_1 approaches 1. The trend in the data with respect to x_1(seen in Fig. 9) is consistent with these limits.

In Fig. 9, the effect of varying J_{L1}, at a fixed J_{G1} on the data can be assessed by looking at data sets S3 and S4. It can be seen that as J_{L1} increases, the data line (or curve) moves around the point (0.5, 0.5) in a clockwise direction. The effect of varying J_{G1}, at a fixed J_{L1}, on the data can be assessed by looking at data sets S1, S2, and S3. It can be seen that as J_{G1} increases, the data line (or curve) moves around the point (0.5, 0.5) in a counter-clockwise direction. This effect is the exact opposite of the effect of increasing J_{L1}. Also, these effects are consistent with the trend seen in the data in connection with x_1. These observed effects of J_{G1} and J_{L1} are consistent with the observations made on the data of other researchers, which were reported by El-Shaboury et al. (2001).

Fig. 10 shows the phase-distribution data for the wavy and stratified-wavy flow regimes. It can be seen that for data set SW with an inlet quality of 0.87, there is a preference for the gas phase to exit through outlet 3 over the range $0.0 < W_3/W_1 < 0.5$. Data set W1 with an inlet quality of 0.64 shows essentially an even phase split over the whole range of W_3/W_1. For data set W2 with an inlet quality of 0.31, there is a preference for the

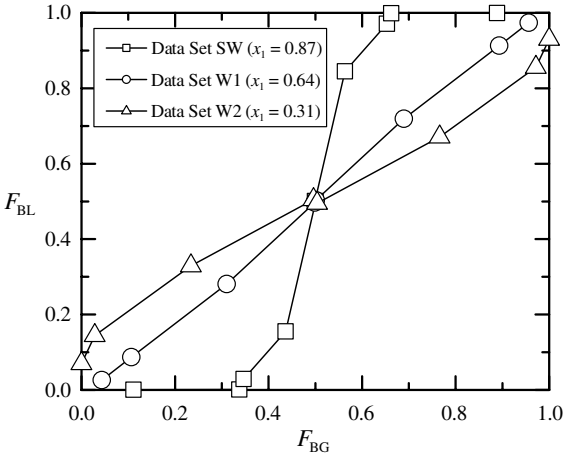

Fig. 10. Phase-distribution data for the wavy and stratified-wavy flow regimes.

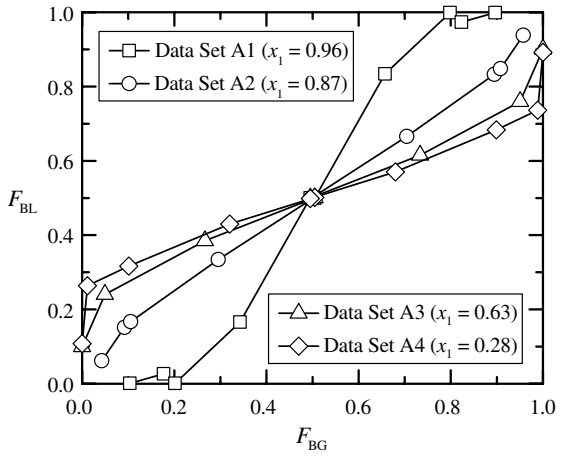

Fig. 11. Phase-distribution data for the annular flow regime.

liquid phase to exit through outlet 3 over the range $0.0 < W_3/W_1 < 0.5$. It can be noted that there is a continuous trend in the data such that as x_1 increases, the data line (or curve) moves around the point (0.5, 0.5) in a counter-clockwise direction. The three data sets shown in Fig. 10 have a J_{G1} of 10 m/s. Thus, the effect of J_{L1}, at a fixed J_{G1}, on the data can be assessed by examining the three data sets. It is clear that increasing J_{L1} results in turning the data line (or curve) around point (0.5, 0.5) in a clockwise direction. All the observations made on Fig. 10 are consistent with those made on Fig. 9 for the stratified flow regime.

The data for sets S1 and W2, both with $x_1 = 0.31$, would essentially lie one over the other on coordinates of F_{BL} versus F_{BG} (as in Figs. 9 and 10). It can be seen then from these two figures that the data are systematic and rotate about (0.5, 0.5) in a counter-clockwise direction with increasing inlet quality.

Fig. 11 shows the phase-distribution data for the annular flow regime. The figure shows that for data set A1, where $x_1 = 0.96$, there is a preference for the gas phase to exit through outlet 3 over the range $0.0 < W_3/W_1 < 0.5$. For data sets A2, A3, and A4 with inlet qualities of 0.87, 0.64, and 0.28, respectively, there is a preference for the liquid phase to go through outlet 3 over the range $0.0 < W_3/W_1 < 0.5$. Fig. 11 also shows that there is a continuous trend in the data such that as x_1 increases, the data line (or curve) moves around the point (0.5, 0.5) in a counter-clockwise direction. As the four data sets shown in Fig. 11 have a J_{G1} of 40 m/s, the effect of varying x_1 may be viewed as the effect of varying J_{L1} at a fixed J_{G1}. These trends in the annular-flow data (in terms of the effects of x_1 and J_{L1}) are consistent with the trends seen in Figs. 9 and 10 for the stratified and wavy flow regimes, respectively.

Comparisons were made between a segment of the present phase-distribution data and data from previous studies (Ottens et al., 1995; Hong and Griston, 1995; Azzopardi et al., 1986a) under the condition of similar inlet conditions. These comparisons included data with inlet flow regimes of stratified-wavy, wavy, and annular. Very good agreement in magnitude and trend were found in these comparisons (El-Shaboury, 2005).

4. Modelling and comparisons

4.1. Pressure-drop correlation

From energy considerations, the pressure drop experienced by the gas phase from the inlet to outlet 3 of the junction can be expressed as

$$\Delta P_{13} = \frac{\rho_G}{2}(V_{G3}^2 - V_{G1}^2) + K_{G,13}\frac{\rho_G}{2}V_{G1}^2 \tag{4}$$

where the first term on the right hand side of Eq. (4) represents the reversible component and the second term represents the irreversible component of the pressure drop. In Eq. (4), V_G is the average gas velocity, and $K_{G,13}$ is the inlet-to-outlet 3 mechanical-energy loss coefficient for the gas phase.

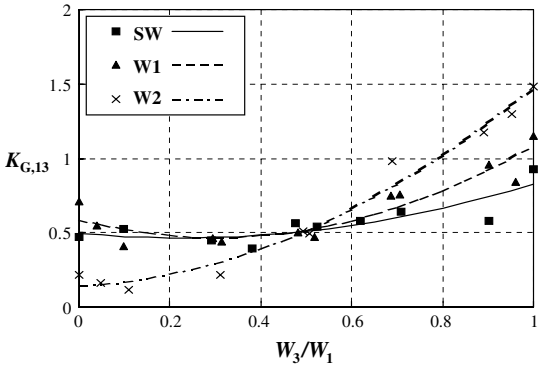

Fig. 12. Values of $K_{G,13}$ for the wavy and stratified-wavy flows.

The average gas velocity V_G was calculated from the following equation:

$$V_{Gi} = \frac{W_{Gi}}{\rho_G \alpha_i A}, \quad i = 1, 2, 3 \tag{5}$$

where A is the cross-sectional area of the pipe and α is the void fraction calculated using the model of Shoham et al. (1987). There is certainly a large number of theoretical models and empirical correlations available in the literature for calculating the void fraction. One advantage of the Shoham et al. models is that they are flow-regime specific, in which case one would expect more accurate predictions relative to models and correlations that are flow-regime independent.

The current data, together with Eq. (4), were used to determine values of the gas-phase mechanical-energy loss coefficient, $K_{G,13}$. A sample of these results is shown in Fig. 12 for wavy flow. Fig. 12 shows that $K_{G,13}$ versus W_3/W_1 follows approximately a parabolic curve for each inlet condition. The curves seen in Fig. 12 passing through the experimental data are parabolas that were obtained by least-square fitting of the experimental data.

Based on the results shown in Fig. 12 and others for annular flow (El-Shaboury, 2005), we can write

$$K_{G,13} = C_1 + C_2(W_3/W_1) + C_3(W_3/W_1)^2 \tag{6}$$

For single-phase flow, the coefficients in Eq. (6) are independent of fluid properties and flow rate, as confirmed by the present results and other data in the literature. However, for two-phase flow, these coefficients appear to depend on the flow regime and the flow rate within the flow regime. For both the wavy and annular flow regimes, C_1, C_2, and C_3 are assumed to be functions of an inlet Reynolds number, Re_1, defined as follows:

$$Re_1 = \frac{4W_1}{\pi D_1 \mu_G} \tag{7}$$

The data of stratified-wavy and wavy flows were found to correlate well with the following equations:

$$C_1 = -4.5688[\log(Re_1)]^2 + 43.569[\log(Re_1)] - 103.28 \tag{8}$$

$$C_2 = 14.469[\log(Re_1)]^2 - 139.51[\log(Re_1)] + 335.44 \tag{9}$$

$$C_3 = -11.424[\log(Re_1)]^2 + 112.14[\log(Re_1)] - 273.69 \tag{10}$$

For annular flow, the following equations were found to give good correlations for the coefficients C_1, C_2, and C_3:

$$C_1 = 0.1908[\log(Re_1)]^2 - 2.9917[\log(Re_1)] + 10.924 \tag{11}$$

$$C_2 = 1.6012[\log(Re_1)]^2 - 20.249[\log(Re_1)] + 63.446 \tag{12}$$

$$C_3 = 9.1961[\log(Re_1)]^2 - 89.465[\log(Re_1)] + 215.72 \tag{13}$$

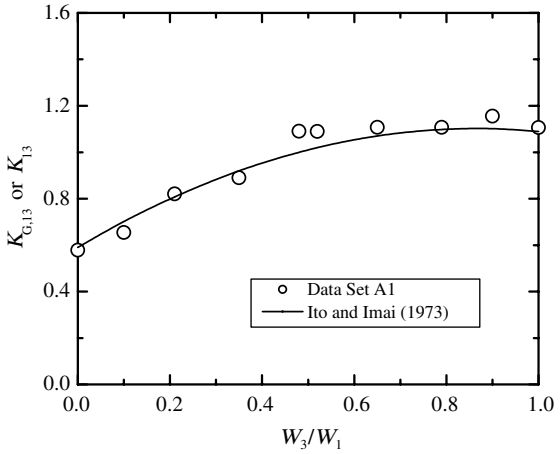

Fig. 13. Comparison between $K_{G,13}$ for data set A1 and the correlation of Ito and Imai (1973).

Fig. 13 shows a comparison between values of $K_{G,13}$ obtained in the current study for data set A1 and the correlation for K_{13} developed by Ito and Imai (1973) for single-phase flow. Data set A1 was selected because it corresponds to a high inlet quality ($x_1 = 0.964$), which is close to single-phase gas flow. The correlation of Ito and Imai is shown over the whole range of W_3/W_1, rather than the range $0.2 \leqslant W_3/W_1 \leqslant 0.8$ recommended by the authors in order to facilitate the present comparison. Fig. 13 shows that the values of $K_{G,13}$ for data set A1 and the correlation of Ito and Imai are in very good agreement.

For the symmetry of an equal-sided horizontal impacting junction to be satisfied, the following equation applies for the same inlet conditions:

$$\Delta P_{12}|_{W_2/W_1=\delta} = \Delta P_{13}|_{W_3/W_1=\delta} \tag{14}$$

Eq. (14) implies that ΔP_{12} can be obtained from Eq. (4) by replacing the outlet-3 parameters with outlet-2 parameters, i.e.,

$$\Delta P_{12} = \frac{\rho_G}{2}(V_{G2}^2 - V_{G1}^2) + K_{G,12}\frac{\rho_G}{2}V_{G1}^2 \tag{15}$$

where

$$K_{G,12} = C_1 + C_2(W_2/W_1) + C_3(W_2/W_1)^2 \tag{16}$$

and coefficients C_1, C_2, and C_3 are as determined above.

The calculated values of ΔP_{13} and ΔP_{12} based Eqs. (4) and (15) were compared with the current experimental data. In these comparisons, the predicted (calculated) values were obtained using the measured values for the phase distribution. It was found that most of the predicted values of ΔP were within $\pm 20\%$ of the corresponding measured values for both wavy and annular flows (El-Shaboury, 2005).

4.2. Modelling of phase distribution

4.2.1. Model equations

For steady, two-phase flow in a horizontal impacting tee with known geometry (D_1, D_2, and D_3) and known fluid properties (ρ_L, ρ_G, μ_L, and μ_G), the remaining parameters are: the mass flow rates (W_1, W_2, and W_3), qualities (x_1, x_2, and x_3), and pressure drops (ΔP_{12} and ΔP_{13}). In practical applications, three parameters are specified (e.g., W_1, x_1, and W_3). In order to determine the remaining five unknown parameters, five equations are required.

From an overall mass balance, we get the first equation

$$W_1 = W_2 + W_3 \tag{17}$$

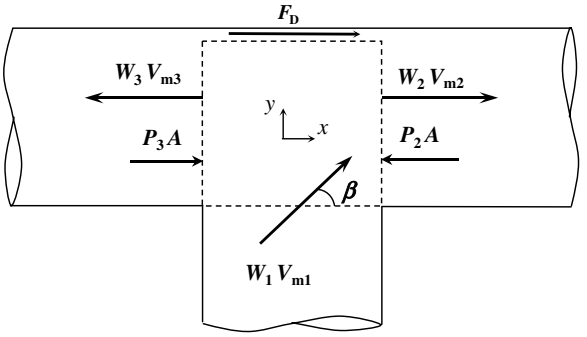

Fig. 14. Momentum-balance parameters at the junction.

A mass balance on the gas phase gives the second equation

$$x_1 W_1 = x_2 W_2 + x_3 W_3 \tag{18}$$

Eq. (4), expressing the energy balance between the inlet and outlet 3 for the gas phase, will be used as the third equation. The fourth equation is an energy balance between the inlet and outlet 2 for the gas phase obtained through symmetry as given by Eq. (15). The fifth equation of the proposed model is the momentum-balance equation at the junction. Fig. 14 shows a control volume situated at the junction with the relevant momentum rates and forces indicated at the control surfaces. In the figure, the parameter F_D is the net drag force acting on the wall of the control volume and V_m is the momentum velocity of the mixture to be defined later. The force F_D can be positive or negative depending on the value of W_3/W_1. Due to symmetry, when $W_3/W_1 = 0.5$, F_D must be equal to zero.

The results of a previous numerical study on single-phase flow in two-dimensional impacting junctions (El-Shaboury et al., 2003) indicate that as the inlet flow approaches the junction, the streamlines deviate from the y-direction. The net effect of the inlet-flow deviation from the y-direction is accounted for by the momentum term $W_1 V_{m1} \cos\beta$ in the x-direction. For $W_3/W_1 = 0.5$, β was set equal to 90° and thus, the net effect of the inlet-flow deviation from the y-direction is zero (as expected) at even mass split. The momentum rates for the flows in outlets 2 and 3 in the x-direction are $W_2 V_{m2}$ and $W_3 V_{m3}$, respectively.

Applying a simple momentum balance in the x-direction on the control volume of Fig. 14, we get

$$P_3 A + F_D - P_2 A = W_2 V_{m2} - W_3 V_{m3} - W_1 V_{m1} \cos\beta \tag{19}$$

where V_m is the momentum velocity of the mixture defined as

$$V_{mi} = \frac{W_i}{\rho_{mi} A}, \quad i = 1, 2, 3 \tag{20}$$

ρ_m is the momentum-weighted density defined as

$$\rho_{mi} = \left[\frac{(1 - x_i)^2}{(1 - \alpha_i)\rho_L} + \frac{x_i^2}{\alpha_i \rho_G} \right]^{-1}, \quad i = 1, 2, 3 \tag{21}$$

and α is the void fraction. The force F_D may be expressed in the following form:

$$F_D = A_w C_f (\rho_{m1} V_{m1}^2)/2, \tag{22}$$

where C_f is a friction coefficient and A_w is the wall area of the control volume, i.e., the area of a cylinder of diameter D and length D less an area A_{CO} cut out of the cylinder by virtue of the intersection with the inlet pipe. Thus,

$$A_w = \pi D^2 - A_{CO} \tag{23}$$

The parameter A_{CO} can be expressed as

$$A_{CO} = a\frac{\pi}{4}D^2 \tag{24}$$

where a is a constant. Eq. (23) can then be written as

$$A_w = (4-a)\frac{\pi}{4}D^2 \tag{25}$$

Substituting the expression for A_w into Eq. (22) and rearranging gives

$$F_D = \frac{\pi}{4}D^2\rho_{m1}V_{m1}\left[\frac{(4-a)}{2}C_f V_{m1}\right] \tag{26}$$

Using Eq. (20), Eq. (26) can be re-written as

$$F_D = W_1 V_{m1}\left[\frac{(4-a)}{2}C_f\right] \tag{27}$$

Substituting in Eq. (19) and rearranging yields

$$(\Delta P_{12} - \Delta P_{13})A = W_2 V_{m2} - W_3 V_{m3} - W_1 V_{m1}\cos\beta - W_1 V_{m1}\left[\frac{(4-a)}{2}C_f\right] \tag{28}$$

The formulations for the angle β and the friction coefficient C_f have to be determined empirically. In order to reduce the empiricism in the proposed model, it was decided to sum up the effects of the friction forces and the deviations from the main directions in one term only as follows:

$$(\Delta P_{12} - \Delta P_{13})A = W_2 V_{m2} - W_3 V_{m3} - W_1 V_{m1}\beta' \tag{29}$$

where $\beta' = \cos\beta + \frac{(4-a)}{2}C_f$.

The five equations comprising the proposed model are Eqs. (4), (15), (17), (18), and (29). Coefficient β' in Eq. (29) needs to be determined.

4.2.2. Determination of the coefficient β'

The measured phase-distribution data and the calculated pressure drops using Eqs. (4) and (15) were substituted in Eq. (29) in order to determine the coefficient β'. Eqs. (8)–(10) obtained originally for the stratified-wavy and wavy flows were also used for stratified flow. Values of β' thus obtained are shown in Fig. 15 for stratified flow; the corresponding results for wavy and annular flows are available in El-Shaboury (2005). The data points that corresponded to values of F_{BG} or F_{BL} less than 0.05 or higher than 0.95 were not included in Fig. 15 because of the higher experimental uncertainty in these points. Fig. 15 shows that β' versus W_3/W_1 follows a nearly linear relation for each inlet condition and therefore, straight lines were fitted through the

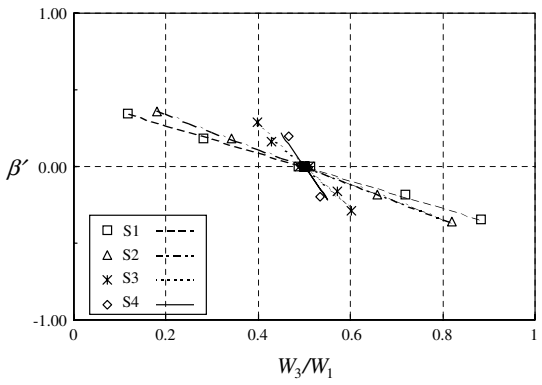

Fig. 15. Values of β' for stratified flow.

data using a least-squares analysis. The figure also shows that for all the inlet conditions, β' is approximately zero at $W_3/W_1 = 0.5$. This is expected according to the definition of β'.

The straight lines fitted through the data in Fig. 15 have the following form:

$$\beta' = Y(W_3/W_1 - 0.5) \tag{30}$$

where Y is the slope of the straight line. The following set of correlations was obtained for the slope Y:

For the stratified flow regime

$$Y = -1.3137(\log(\dot{M}_R Re_1 x_1))^2 + 11.94(\log(\dot{M}_R Re_1 x_1)) - 27.696 \tag{31}$$

For the stratified-wavy and wavy flow regimes

$$Y = -0.5347(\log(\dot{M}_R Re_1))^2 + 6.5693(\log(\dot{M}_R Re_1)) - 19.63 \tag{32}$$

and for the annular flow regime

$$Y = 11.735(\log(Re_1^{1.5} x_1^{0.8}))^3 - 263.44(\log(Re_1^{1.5} x_1^{0.8}))^2 + 1971.4(\log(Re_1^{1.5} x_1^{0.8})) - 4918.38 \tag{33}$$

where Re_1 is an inlet Reynolds number given by Eq. (7) and $\dot{M}_R$ is the inlet-momentum-flux ratio defined as follows:

$$\dot{M}_R = \rho_G V_{G1}^2 / \rho_L V_{L1}^2 \tag{34}$$

where V_{G1} and V_{L1} are the average inlet velocities of the gas and the liquid, respectively, given by $V_{G1} = \frac{W_1 x_1}{\rho_G A \alpha_1}$ and $V_{L1} = \frac{W_1(1-x_1)}{\rho_L A(1-\alpha_1)}$ with α determined from the model of Shoham et al. (1987).

4.2.3. Comparison between the proposed model and experimental data

Comparisons were made between the predictions of the above model and experimental data from the present investigation and others from the literature. In executing the model, the experimental values of W_1, x_1, and W_3 were used as input, and the corresponding values of W_2, x_2, x_3, ΔP_{12}, and ΔP_{13} were obtained from the model. Values of F_{BG} and F_{BL} used in the comparisons were calculated from $F_{BG} = W_3 x_3/(W_1 x_1)$ and $F_{BL} = W_3(1 - x_3)/[W_1(1 - x_1)]$, respectively. A sample of these comparisons is presented here and many more results can be found in El-Shaboury (2005).

The comparison with the present data of wavy flow can be seen in Fig. 16 for the pressure drop and Fig. 17 for the phase distribution. Fig. 16 shows good agreement between the predictions and the data with 73% of the data predicted within ±20% while 83% of the data were predicted within ±30%. As well, good agreement in magnitude and trend can be seen in Fig. 17 for the phase distribution.

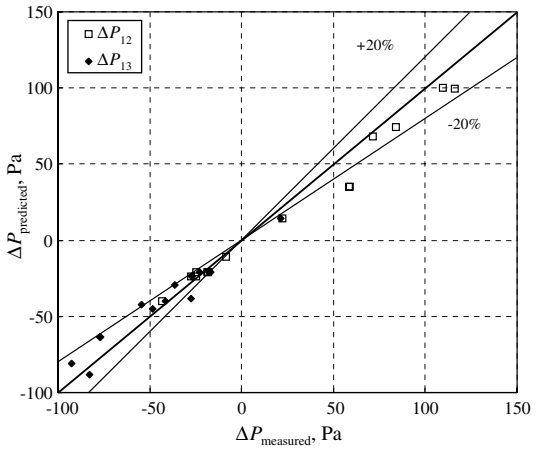

Fig. 16. Comparison of measured and predicted values of ΔP for stratified-wavy and wavy flows.

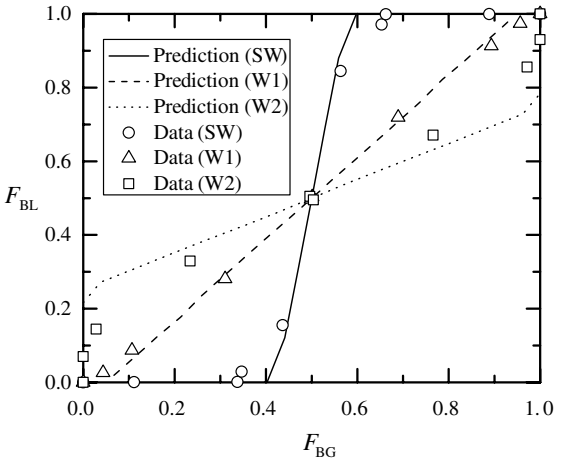

Fig. 17. Phase-distribution predictions by the current model against the current data for stratified-wavy and wavy flows.

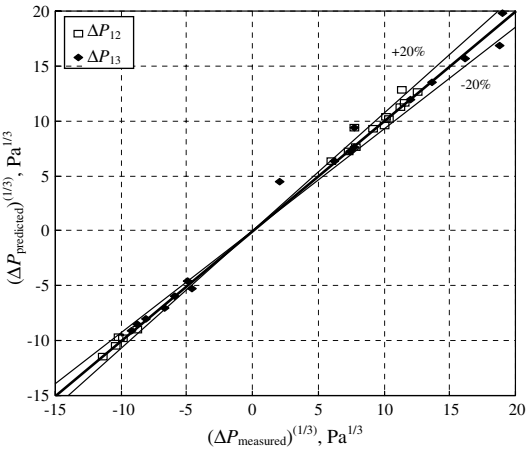

Fig. 18. Comparison of measured and predicted values of ΔP for annular flow.

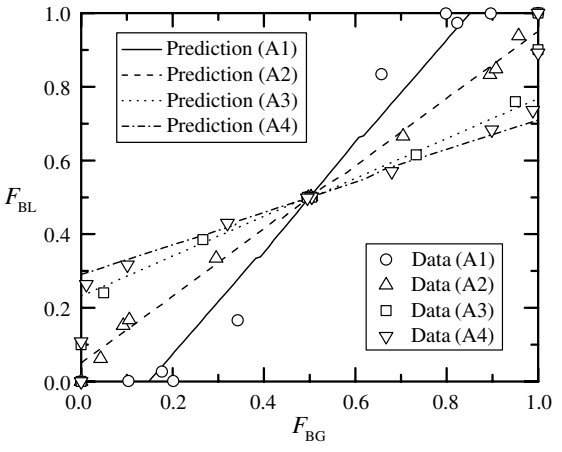

Fig. 19. Phase-distribution predictions by the current model against the current data for annular flow.

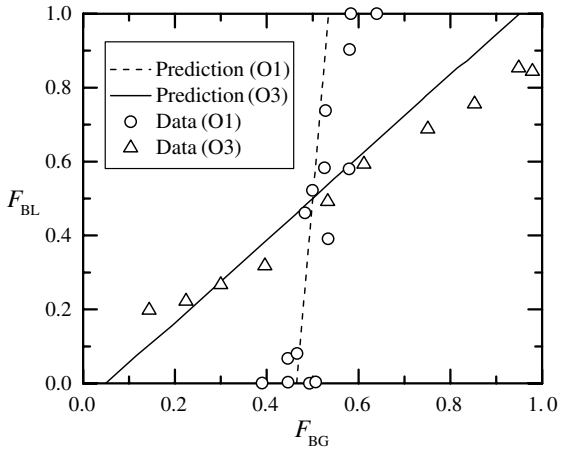

Fig. 20. Phase-distribution predictions by the current model against wavy-flow data from Ottens et al. (1995).

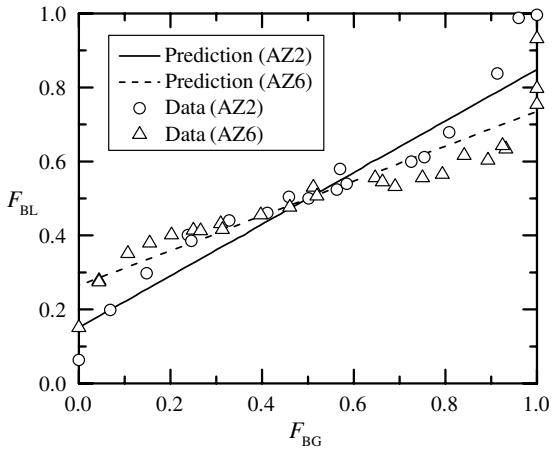

Fig. 21. Phase-distribution predictions by the current model against annular-flow data from Azzopardi et al. (1986a).

The comparison with the present data of annular flow can be seen in Fig. 18 for the pressure drop and Fig. 19 for the phase distribution. Fig. 18 shows good agreement between the predictions and the data with 79% of the data predicted within ±20% while 85% of the data were predicted within ±30%. As well, Fig. 19 shows good agreement between the predictions and the data in terms of magnitude and trend.

Fig. 20 shows a comparison between the present model and the phase-distribution data of wavy flow from Ottens et al. (1995). The two data sets shown in the figure correspond to $J_{G1} = 15.8$ m/s with $J_{L1} = 0.00063$ m/s for set O1 and $J_{L1} = 0.012$ m/s for set O3. In terms of magnitude, Fig. 20 shows reasonable agreement between the predictions and the data and the trends seen in the predictions are consistent with the expected effect of varying J_{L1}. No pressure-drop data were reported in the work by Ottens et al.

Fig. 21 shows the current phase-distribution predictions against phase-distribution data from Azzopardi et al. (1986a) for annular flow in an impacting tee with a vertical inlet. The two data sets shown in the figure are marked AZ2 (with inlet conditions $J_{L1} = 0.0317$ m/s and $J_{G1} = 17.55$ m/s) and AZ6 (with inlet conditions $J_{L1} = 0.079$ m/s and $J_{G1} = 15.96$ m/s). Fig. 21 shows a reasonable agreement between the predictions and the data in terms of magnitude. As well, data sets AZ2 and AZ6 have different values of J_{L1} while values of J_{G1} are close. Fig. 21 shows that the data, as well as the predictions, follow the expected trend for varying J_{L1}.

5. Conclusions

An experimental investigation was conducted to generate phase-distribution and pressure-drop data for air–water flows in a horizontal impacting tee junction with equal-diameter sides and a system pressure of 1.5 bar. The data corresponded to inlet flow regimes of stratified, wavy and annular. A model capable of predicting the phase distribution and pressure drop was developed. The model predictions were compared against the current data as well as the phase-distribution data of other researchers. Based on the current results and the aforementioned comparisons, the following conclusions can be drawn:

- In general, even phase split is obtained only at even mass split.
- At a fixed J_{L1}, and within the same flow regime, the data line (or curve) moves around the point (0.5, 0.5) on an F_{BL}–F_{BG} graph in a counter-clockwise direction as J_{G1} increases. This effect is the exact opposite of the effect of increasing J_{L1} at a fixed J_{G1}. These effects of varying J_{G1} and J_{L1} were found to be consistent in the current data and the data of other researchers for horizontal impacting junctions. Also, these effects of J_{L1} and J_{G1} on the phase distribution were found to be valid within each inlet flow regime. The effect of varying the inlet quality x_1 on the phase-distribution data can be easily deduced using the aforementioned effects of varying J_{G1} and J_{L1}.
- Based on observations on the current phase-distribution data, the effects of varying J_{G1}, J_{L1}, and x_1 mentioned above were found to be continuous within the stratified and wavy flow regimes. However, these effects were found not to be continuous at the boundary between wavy and annular flow regimes.
- In general, the value of ΔP_{13} increases with the split ratio W_3/W_1 and the absolute value of ΔP_{13} increases with the inlet mass flow rate W_1.
- For annular flows, the magnitudes of ΔP_{13} are much greater than those for wavy and stratified flows (Even though for stratified flow, values of ΔP_{13} were not reported in the current study, it is thought that the part of the aforementioned conclusion regarding stratified flows, is true).
- For stratified flow, a change in the level of the gas–liquid interface occurs in the inlet pipe. This change in the level of the interface might also occur in the two outlets of the junction. These changes in the levels of the interfaces have significant effects on the magnitude of the pressure-distribution data for stratified flow. Any changes in the interface levels were found to be insignificant for ΔP in wavy and annular flows.
- A model capable of predicting the phase distribution and pressure drop in horizontal, equal-sided, impacting tee junctions was developed. The model has been tested for air–water systems at pressures ranging from 1.0 to 1.7 bar, with junction diameters ranging from 19 to 37.8 mm, and for the three inlet flow regimes of stratified, wavy, and annular. In general, comparisons between the model predictions and the current phase-distribution data, as well as data of other researchers, showed good agreement in magnitude and trend. Also, the model predicted the current pressure-drop data within $\pm 30\%$ for 85% of the annular-flow data and 83% of the data of stratified-wavy and wavy flows.

Acknowledgement

The financial support provided by the Natural Sciences and Engineering Research Council of Canada is gratefully acknowledged.

References

Asano, H., Fujii, T., Takenaka, N., Sakoda, K., Arakawa, T., 1997. Phase separation characteristics of gas–liquid two-phase flow in a T-junction (experiments for a one-component two-phase flow). In: Proceedings of the 16th Multiphase Flow Symposium, Lake Toya, Japan, pp. 103–104.

Azzopardi, B.J., Purvis, A., Govan, A.H., 1986a. Two-phase flow split at an impacting T. UKAEA Report, AERE-R-12179.

Azzopardi, B.J., Purvis, A., Govan, A.H., 1986b. Flow split of churn flow at a vertical impacting T. UKAEA Report, AERE-R-12440.

Azzopardi, B.J., 1999. Phase separation at T junctions. Multiphase Sci. Technol. 8, 645–714.

Buell, J.R., Soliman, H.M., Sims, G.E., 1994. Two-phase pressure drop and phase distribution at a horizontal tee junction. Int. J. Multiphase Flow 20, 819–836.

Chien, S.F., Rubel, M.T., 1992. Phase splitting of wet steam in annular flow through a horizontal impacting tee. SPE Prod. Eng. 7, 368–374.

Chisholm, D., 1967. A theoretical basis for the Lockhart–Martinelli correlation for two-phase flow. Int. J. Heat Mass Transf. 10, 1767–1778.

El-Shaboury, A.M.F., 2005. Phase distribution and pressure drop of two-phase flows in a horizontal impacting tee Junction. Ph.D. Thesis, University of Manitoba, Canada.

El-Shaboury, A.M.F., Soliman, H.M., Sims, G.E., 2001. Current state of knowledge on two-phase flow in horizontal impacting tee junctions. Multiphase Sci. Technol. 13, 139–178.

El-Shaboury, A.M.F., Soliman, H.M., Ormiston, S.J., 2003. Laminar forced convection in two-dimensional impacting tee junctions. Heat Mass Transf. 39, 815–824.

Fujii, T., Takenaka, N., Nakazawa, T., Asano, H., 1995. The phase separation characteristics of gas–liquid two-phase flow in the impacting T-junction. In: Proceedings of the 2nd International Conference on Multiphase Flow, Kyoto, Japan, pp. 6.27–6.32.

Grolman, E., Fortuin, J.M.H., 1997. Liquid hold-up, pressure gradient, and flow patterns in inclined gas–liquid pipe flow. Exp. Therm. Fluid Sci. 15, 174–182.

Hong, K.C., 1978. Two-phase flow splitting at a pipe tee. J. Petrol. Technol. 2, 290–296.

Hong, K.C., Griston, S., 1995. Two-phase flow splitting at an impacting tee. SPE Prod. Facil. 10, 184–190.

Hwang, S.T., 1986. A study on phase separation phenomena in branching conduits. Ph.D. Thesis, Rensselaer Polytechnic Institute, NY.

Hwang, S.T., Soliman, H.M., Lahey, R.T., 1989. Phase separation in impacting wyes and tees. Int. J. Multiphase Flow 15, 965–975.

Ito, H., Imai, K., 1973. Energy losses at 90° pipe junctions. J. Hydr. Div. ASCE 99 (paper no. HY9), 1353–1368.

Kline, S.J., McClintock, F.A., 1953. Describing the uncertainties in single-sample experiments. Mech. Eng. 75, 3–8.

Lockhart, R.W., Martinelli, R.C., 1949. Proposed correlation of data for isothermal two-phase, two-component flow in pipes. Chem. Eng. Prog. 45, 39–48.

Mandhane, J.M., Gregory, G.A., Aziz, K., 1974. A flow pattern map for gas–liquid flow in horizontal pipes. Int. J. Multiphase Flow 1, 537–553.

Moffat, R.J., 1988. Describing the uncertainties in experimental results. Exp. Therm. Fluid Sci. 1, 3–17.

Ottens, M., De Swart, A., Hoefsloot, H.C.J., Hamersma, P.J., 1995. Gas-liquid flow splitting in regular, reduced and impacting tee junctions. Impiantistica Ital. 8, 23–33.

Shoham, O., Brill, J.P., Taitel, Y., 1987. Two-phase flow splitting in a tee junction- experiment and modelling. Chem. Eng. Sci. 42, 2667–2676.